

Testing of Technical Fabrics under Fast Camera Control

Paweł Kłosowski¹, Krystyna Michałowska¹, Marek Przyborski², Wojciech Jurczak^{3*}

¹ Faculty of Civil and Environmental Engineering, Gdansk University of Technology, ul. Gabriela Narutowicza 11/12, 80-233 Gdańsk, Poland

² Navigation and Naval Weapons Faculty, Polish Naval Academy, Inżyniera Jana Śmidowicza 69, 81-127 Gdynia, Poland

³ Mechanical-Electrical Engineering Faculty, Polish Naval Academy, Inżyniera Jana Śmidowicza 69, 81-127 Gdynia, Poland

* Corresponding author's e-mail: w.jurczak@amw.gdynia.pl

ABSTRACT

The dynamic development of measurement and recording techniques has been changing the way one conceives material strength. In this study, two different methods of evaluating the strength of fabrics are compared. The first is the typical and commonly used technique based on the use of a testing machine. The second method uses the so-called “fast camera” to monitor the entire process of the destruction of a fabric sample and analyse the behaviour of the fabric during the experiment. Both methods provide interesting data and present a very specific way of experimentally evaluating the strength of fabrics.

Keywords: textile fabric, strength tests, rapid phenomenon, fast cameras.

INTRODUCTION

The rapid development of textile structures began in the 1950s [1]. This development is strongly linked to the development of numerical calculation techniques (especially the finite element method [2]) and laboratory testing techniques [3–5]. Laboratory tests are necessary to recognise the type of constitutive relations of different types of fabrics that can be used in finite element analysis. In particular, technical fabrics usually exhibit highly non-linear behaviours, and their properties depend on the direction; that is, these fabrics exhibit anisotropic properties. Therefore, even for engineering applications, laboratory testing techniques are very complex. At the end of the 20th century, the tests were most often performed using typical testing machines. They were usually executed according to European standards, such as that described in [6]. The European standard [6] did not require the test to be conducted using an extensometer, and therefore, only general information on the behaviour

of the tested fabric could be obtained from such tests. An extensometer (especially a video extensometer) provides results of higher quality and enables the identification of non-linear properties, especially the rheological properties, of technical fabrics [7–9]. More complex experiments have been performed using biaxial tensile machines [10–12]. In 2018, the European standard for biaxial tensile tests was developed [10]. Although many investigations have been performed based on this standard, [14] those tests have generally focused on the testing conditions. The subsequent studies in technical fabric engineering were focused on the damage and ageing of fabrics [15], [16]. The application of mechanical testing machines supported by digital image correlation (DIC) systems has enabled the observation of the strain (stress) distribution on the entire surface of the tested fabric [14, 17, 18]. Unfortunately, such tests are usually not supported by high-resolution cameras, but with restricted sampling frequency. Fast cameras can essentially overcome this problem. The usability of these instruments has been

proved in the field of experimental fluid dynamics, where fast cameras play the most important role in the process of decoding the mechanism of turbulence. Recent investigations show that fast cameras may be very useful in research directed to better describing of formulation of human emotions. Speed recording gives a unique insight into the process of occurring facial expressions which can lead to learning computers how to understand humans behaviour.

In this work, the rapid evolution of the damage in the technical fabric is investigated using a fast camera. By using a fast camera and well-known methods of PIV (Particle Image Velocimetry) our group tries to describe dynamics that one can observe on the surface of the tested fabric which can be useful to diagnose the real shape of the fabric.

TECHNICAL FABRICS

Technical fabrics are composite materials widely used in civil engineering. They are generally applied in the construction of hanging roofs, sometimes as frameworks for shells, small independent roofs, etc. They are usually constructed from three groups of materials. Two of them (threads) are two groups of fibres, viz. warp and weft. The third covers the first two and is referred to as the coating (Fig. 1).

Thin fibres are most often made from polyester or glass. The modern coating consists of several material layers for protection against humidity, UV light, and dirt; the main component is however made of polyvinyl chloride (PVC) for polyester fibres or polytetrafluoroethylene PTFE (Teflon) for glass threads. Owing to its complex structure, the technical fabric shows anisotropic properties. Usually, special constitutive models should be used for their analysis using the finite element method [19]. One of the very promising

models is the dense net model [19, 20], which can be used for describing several types of constitutive behaviours (e.g. non-linear elastic, viscoelastic, or viscoplastic behaviours), according to the targeted application. To identify the mechanical properties of the fabric for a specific application using the dense net model, it is necessary to identify the uniaxial properties of the fabric in the warp and weft directions. This simplifies the requirement of experimental equipment that should be used to perform appropriate tests. Additionally, the identification process is in this case also relatively simple [21]. One of the important aspects that should be investigated in the technical analysis of fabric behaviour is the damage mechanism [15, 22]. During typical laboratory experiments, it is difficult to distinguish the origin of the damage, which is the reason for the appearance and propagation of a crack. Such effects can be investigated when a special fast camera is used for recording the test process.

EXPERIMENTAL EQUIPMENT

The tests were performed in the Laboratory of Structural Mechanics of Civil and Environmental Faculty at the Gdańsk University of Technology. The laboratory is equipped with a Z400 Zwick-Roell testing machine. The machine was equipped with a mechanical extensometer and thermal chamber (Fig. 2). It has two force heads: one with 400 kN force and another with 50 kN force. The experiments on technical fabrics were performed in ambient conditions (20 °C, normal humidity) and under the regime described in the ISO standard [21]. Therefore, there was no need to use the thermal chamber or extensometer during the tests. The specimens were fixed in flat grips.

To record the damaging process of the specimen, a fast camera (Phantom Miro) was used.

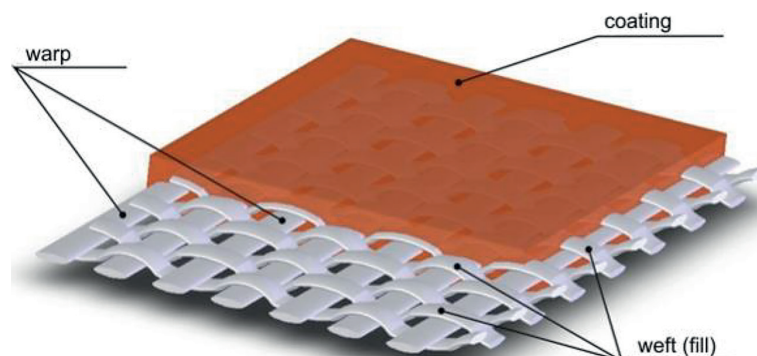


Fig. 1. Construction of a fabric

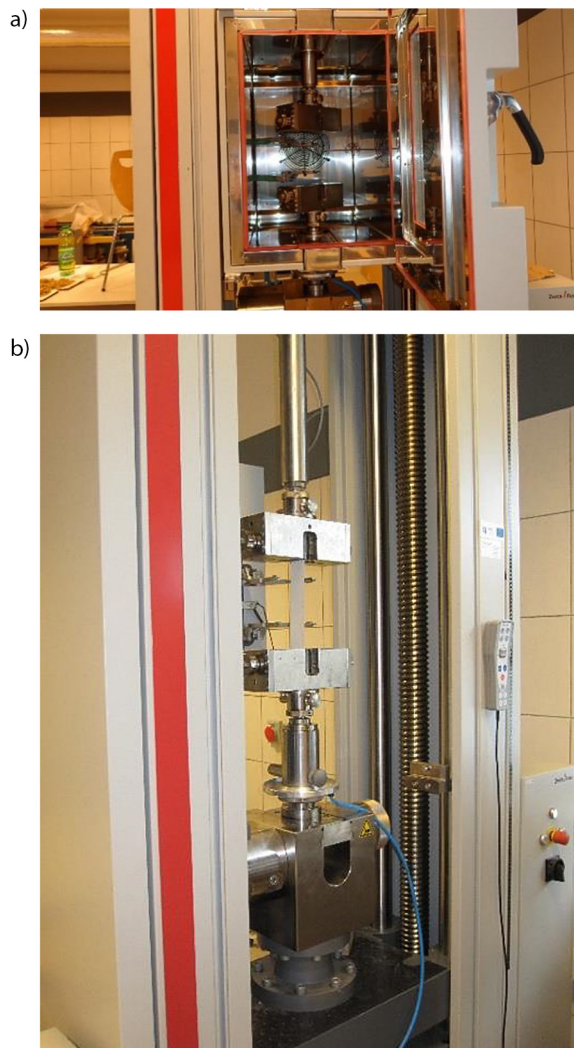


Fig. 2. Testing machine Z400 with an extensometer and thermal chamber (a), photograph captured during a textile fabric test (b)

The numerical results of the experiments (time, displacement, and force) were recorded as ASCII files using a computer. The camera recorded the experimental process using a 12 GB memory buffer, which means that when the buffer is full, the recorded image re-fills the buffer. When the experiment is completed and the trigger is pressed, the image currently in the buffer is saved. In the discussed case, at the recording speed of 57,000 frames per second, there were 235,829 frames for specimen 1, 78610 frames for specimen 2 and 49,564 frames for specimen 3.

SPECIMENS AND TEST PROCEDURE

The specimens were cut from a polyester textile fabric (VALMEX P50 produced by Mehler Technologies) that was used in the construction

of a hanging roof of the Forest Opera in Sopot in 1992 and employed up to 2009 (Fig. 3) [22]. The main mechanical properties of that fabrics are collected in Table 1. In 2009, the roof was replaced by a new one; thus, the old fabric could be used for experiments. In the fast camera tests, the specimens cut from the virgin fabric (unused) were stored for roof repair, and those cut from the fabric used as a roof for several years were used. Here, the results of three tests that best describe the differences in the fabric damage behaviours are presented. All the specimens were cut in the weft direction. They were cut to an active length of 100 mm and width of 50 mm (according to Ref. [23]). As shown in Figure 4, the clamping lengths varied. These differences however did not influence the proper clamping of the specimens. The tests were performed at a constant displacement rate of 100 mm/min.

TEST RESULTS

The strain–stress characteristics during the tests are presented in Figure 5. The strain–stress functions obtained in all the tests are very similar, indicating that the mechanical properties of the fabric were maintained regardless of whether the fabric was exposed to different weather conditions for almost 20 years, or was stored in ideal conditions (dark cellar). As expected, the obtained ultimate force is higher for the specimen that was broken in the middle of its length. This result is consistent with that reported previously [23]. Three screenshots of each test captured using the fast camera are presented in Fig. 6–8. As shown, the point where the crack appears depends strongly on the fixing length between the grips. For a relatively long and both sides equal fixing length, the crack appears in the middle of the specimen, whereas when the fixing length is short, the crack appears close to the short end of the fixed grip.

Further, the crack always began at the edge of the specimen and then propagated to the middle. There is however no indication of this effect in the plot in Figure 5 because the process is very quick when the test is conducted with a displacement rate of 100 mm/min (with a sampling rate of approximately 0.01 s).

The rapid development of imaging techniques has enabled the observation of very fast phenomena. The “high-speed cameras” allow the

Table 1. The main mechanical properties of textile fabric

Material Properties	Unit	Method	Value
Basic material		DIN ISO 2076	Polyester Panama Weave P2/2
Total weight	g/m ²	EN ISO 2286–2	1050
Fabric thickness	mm		~0.9
Yarn count	dtex	ISO 2060	1670
Tensile strength warp/weft	N/50 mm	EN ISO 1421/V1	6000 / 5500
Elongation at break	%	EN ISO 1421/V1	24/32
Tear strength warp/weft	N	DIN 53363	900 / 800

recording of images at very high speeds, and thus enable the observation of phenomena that are invisible to the naked eye. In the following section, we demonstrate how the tests discussed above can be monitored using this type of equipment.

The monitoring of the entire course of the experiment on the film allows us to view and analyse the process of the tearing of the material, whereas, in the case of a testing machine, only the force value and displacement are registered. The distortion that the material sample suffers during the experiment is also important; this can be observed during the reproduction of the recorded phenomenon. At very high registration rates, a comprehensive picture of the phenomenon can be obtained. Using the commonly known and well-developed methods of digital particle image velocimetry (DPIV), which is used in fluid mechanics, it is possible to obtain a broad picture of the changes occurring on the surface of the material during the test. This method in combination with some image processing algorithms can aid obtain

a picture of the surface of a material, which opens a new pathway for analysing the results of the strength tests.

Upon applying edge detection filters, in this case, the Sobel Filter (there is rich information on different filters in the scientific literature, and we only delve into the very broad topic in this study; see discussions in [23–29]), a view of the detected and identified objects on the surface of a material can be obtained. These objects are the characteristic elements that appear in all the frames of the film, and one can track their movement during the experiment. The identified objects of the three specimens are shown in Figure 9. For the first specimen, 364 objects were identified on the image with the specific value of the diameter of the object equalling 6 pixels. For the second specimen, 419 objects were identified, while 611 objects were identified for the third one, as shown in Figure 9.

To obtain meaningful information from the identified objects, first, the series of images must



Fig. 3. Roof of the Forest Opera in Sopot (2009).



Fig. 4. Specimens after tests (No. 1 and 2 are virgin unused fabric, No. 3 is used fabric).

be subjected to certain transformations that allow the detection of characteristic objects on the material surface. These objects can be used to track the evolution or to form the trajectory of the movement of certain points, throughout the experiment. This allows a completely different characterisation of the phenomenon occurring at

the surface of the material. In the present case, owing to the pre-processing of the collected images of all three specimens, it was possible to obtain a view of the trajectories on the surfaces of the specimens. Figure 10 demonstrates the complicated movement of a single object on the specimen surface.

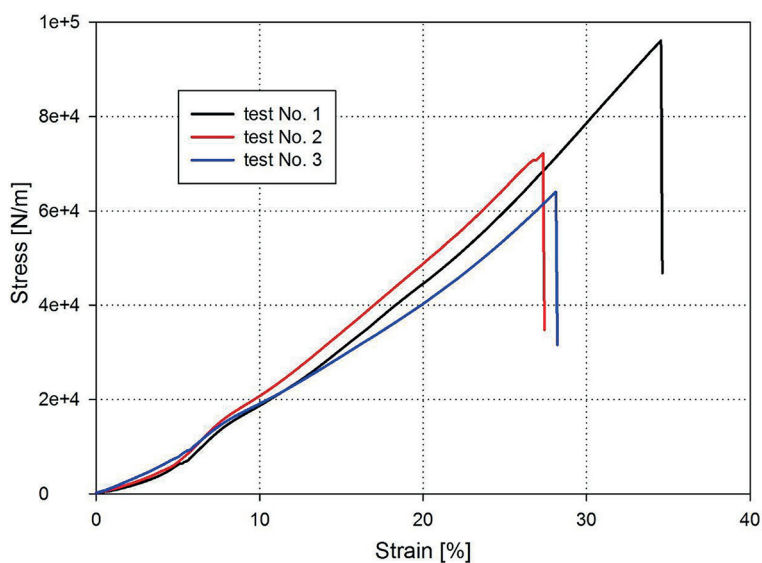


Fig. 5. Experimental strain–stress functions

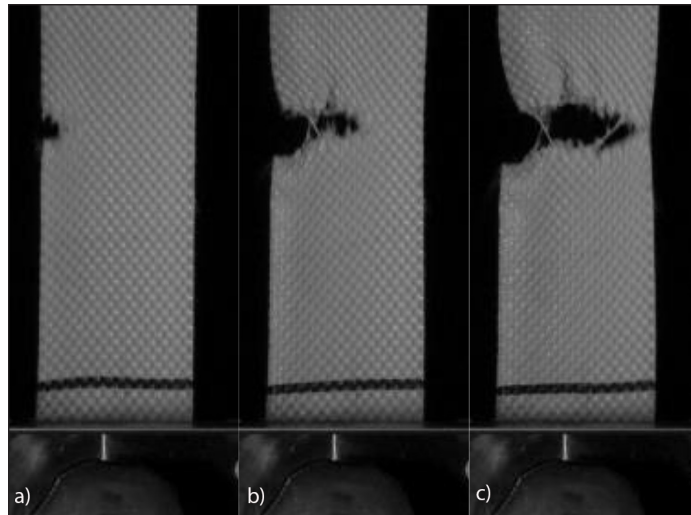


Fig. 6. Damage development in Specimen No. 1.

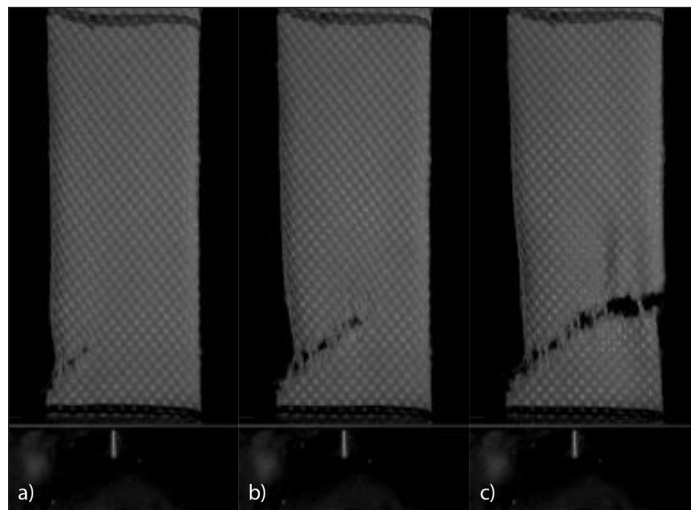


Fig. 7. Damage development in Specimen No. 2.

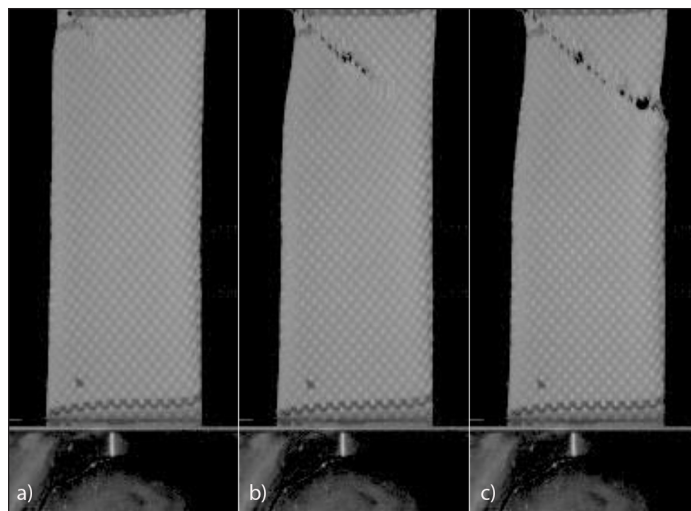


Fig. 8. Damage development in Specimen No. 3.

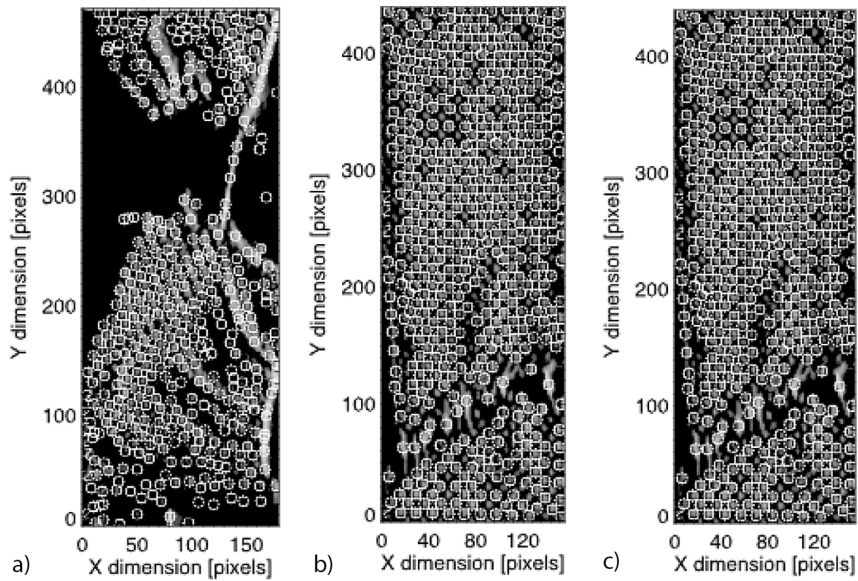


Fig. 9. Objects identified on the surfaces for Specimen No. 1 to 3 (left to right)

By drawing trajectories lasting at least one frame, it is possible to analyse the changes occurring on the surfaces of the specimens in a new way. Figure 10 and Figure 11 show the complexity of the processes occurring on the surface during the tests. We can also select the longest trajectories, that is, trajectories that last from the start of the observation until the end, on the three specimens, as shown in Figure 12.

Tracking allows the calculation of a very important parameter, the dispersion of these objects. The material will not behave like a fluid, and the movements of these objects are limited. Nevertheless, the objects will always disperse, as demonstrated in Figure 13 for the present case. The physical significance of the dispersion in the case of the material being tested corresponds to the displacement in both the *X* and *Y* directions, as shown in Figure 13.

DISCUSSION

Herein, we present some interesting possibilities offered by DPIV in the analysis of the strength of materials. For this analysis, the PIV-Lab toolbox for Matlab (see [30–33]), which is available as free software, was used. The movement of objects detected on the material provides a wide insight into the stretching phenomenon and the related effects during the tests.

In brief, the main idea behind this method is to use a pair of images, for example, A and B recorded at time *t* and *t* + Δt , respectively. Hence, the velocity of the movement of identified objects on the fabric surface can be derived from Δt and the distance the objects travelled can be determined from the two images (this is the displacement). To calculate the displacement, a discrete cross-correlation function can be used, as proposed in [34–36]. The most probable

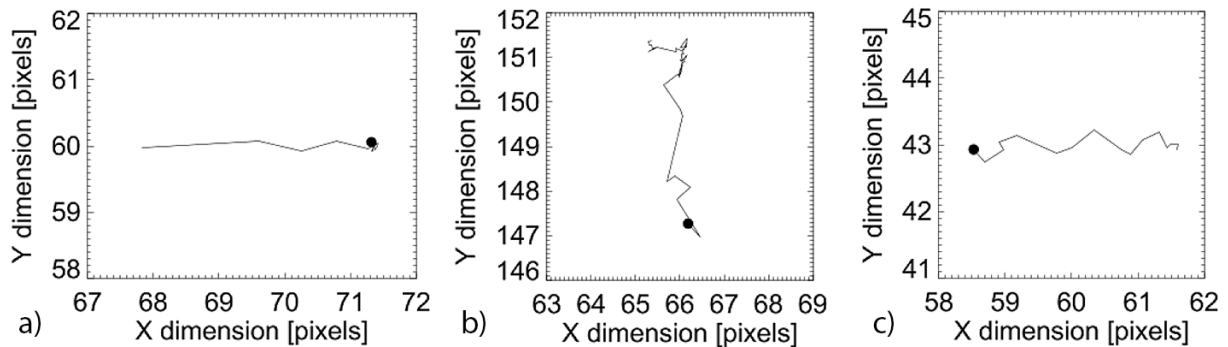


Fig. 10. Examples of the single trajectories of a given object on the specimens: Specimen No. 1 (a), No. 2 (b), and No. 3 (c)

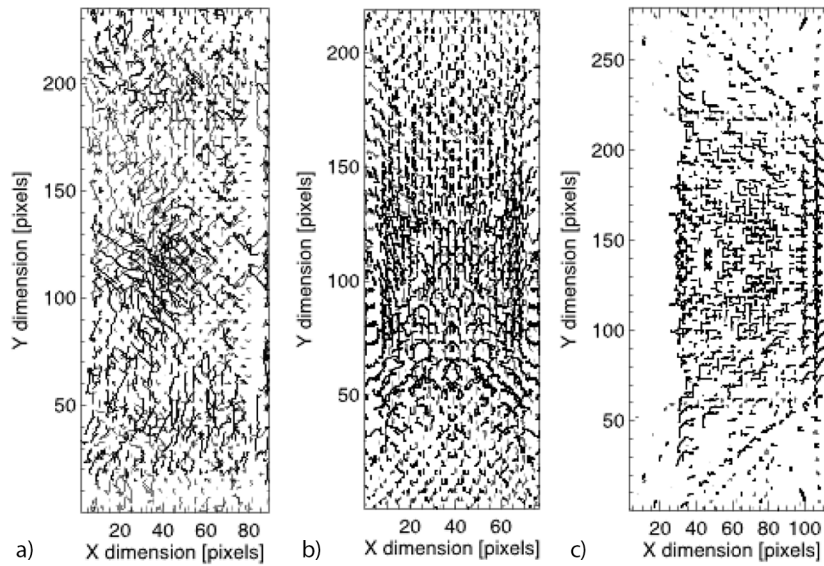


Fig. 11. Trajectories that last at least for 1 frame for Specimen No. 1 (a), No. 2 (b), and No. 3 (c)

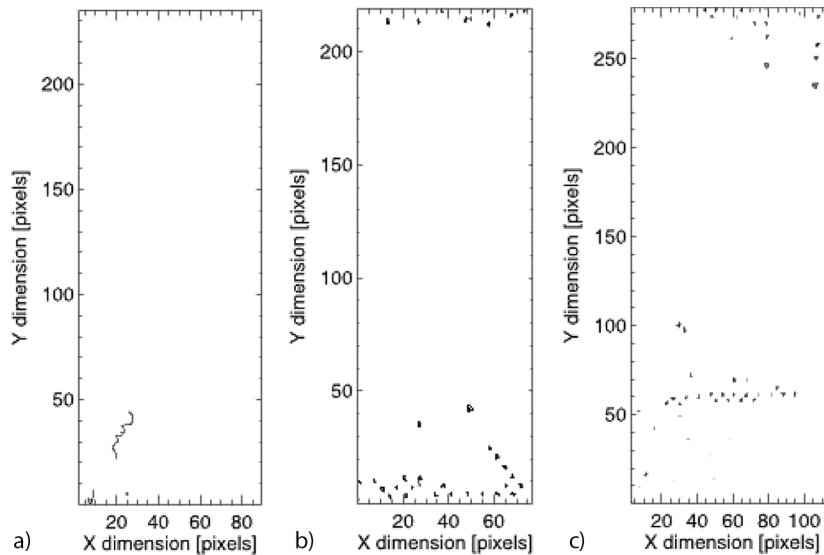


Fig. 12. The longest trajectories on the specimens: Specimen No. 1 (a), No. 2 (b), and No. 3 (c)

displacement is calculated for a group of objects located in the small sub-images referred to as interrogation areas, $A(i,j)$ and $B(i - m,j - n)$. In this case, the sub-images have dimensions of 16×16 pixels. The peak in the cross-correlation $C(m,n)$ (see Eq. (1)) plot represents the average displacement of the object in the interrogation area. The analysis algorithm starts from the upper left corner of the first image, A, and the same position in the second image, B. Then, this 16×16 pixel mask changes its location in each image until it reaches the edge of both images.

$$C(m,n) = \sum_i \sum_j A(i,j)B(i - m,j - n) \quad (1)$$

where: i and j represent the row and column of the interrogation segment in the image, respectively;

m and n represent the row and column of the cross-correlation matrix, respectively.

One of the interesting possibilities of the PIV-Lab toolbox is the access to profiles presented in Figure 14 (red lines).

In fact, one can obtain such profiles for any location on the sample, those presented in Figure 14 were chosen for the presented experiment. Based on these considerations, one may calculate the values of several derivatives. Below, we present some examples of derivatives calculated for the

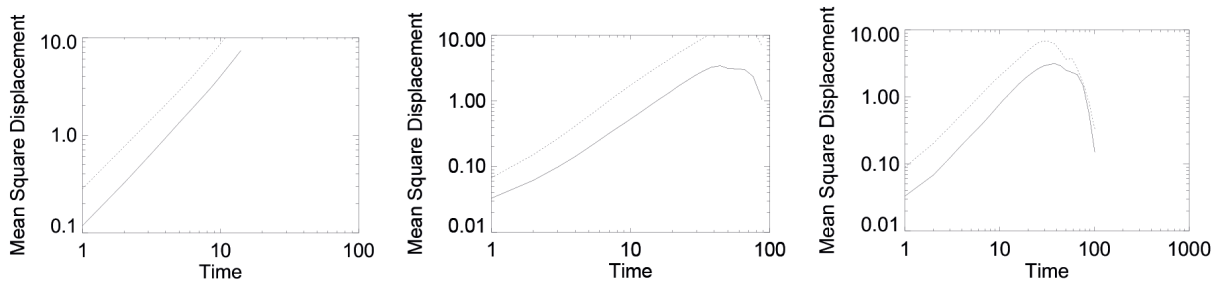


Fig. 13. Mean square displacement calculated for the specimens: Specimen No. 1 (a), No. 2 (b), and No. 3 (c) solid line represent displacement in X direction and the dotted line represents displacement in Y direction

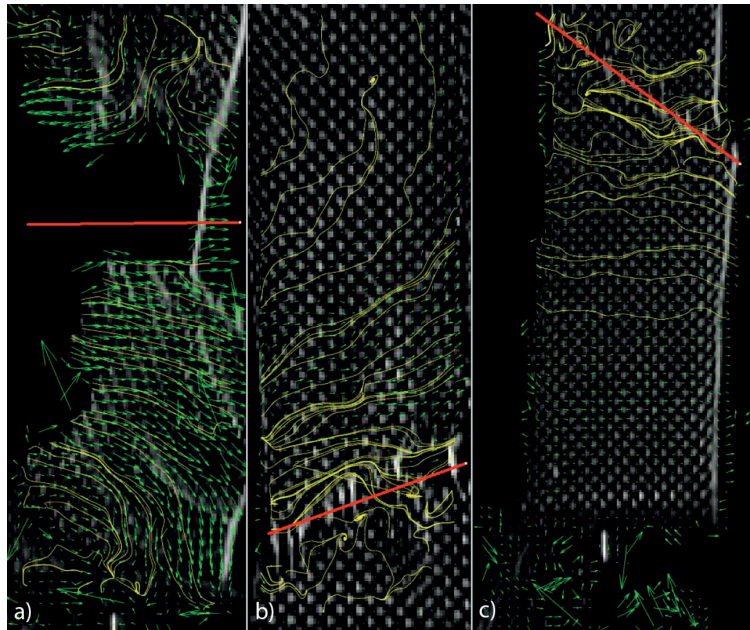


Fig. 14. Profile lines (red) in the specimens: Specimen No. 1 (a), No. 2 (b), and No. 3 (c)

profile lines specified in Figure 14. For example, the velocity magnitude is plotted in Figure 15.

This category gives a brief view of how the velocity of the movement of t grid nodes (see Fig. 14) changes in the particular location shown on the fabric.

Very often, vorticity statistics are used to describe a flow in the field of fluid dynamics (for

example, see [33]). Theoretically, in the core of a vortex, the magnitude of the vorticity is larger than zero; outside the vortex core, the vorticity equals zero (see Fig. 16).

In Ref. [32], a new type of visualisation (see Fig. 20) was proposed, based on releasing streamlines at every grid point of the vector field of the flow. One criterion for a vortex, as presented in

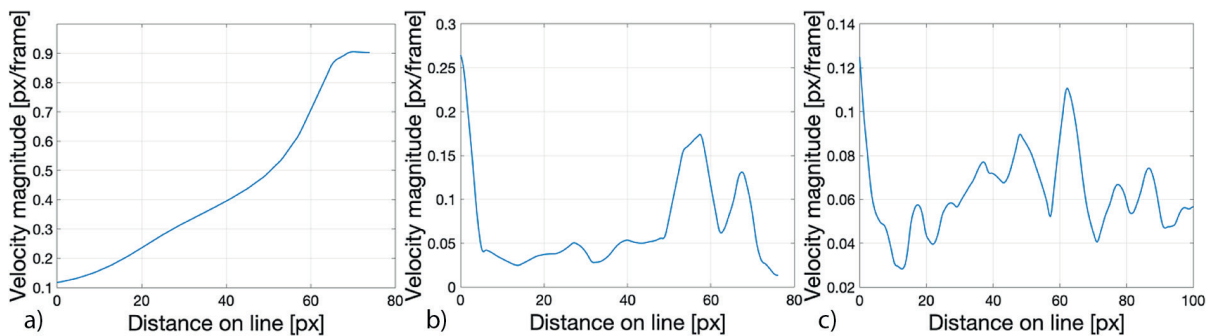


Fig. 15. Velocity magnitude of the movement on the profile lines of the specimens: Specimen No. 1 (a), No. 2 (b), and No. 3 (c)

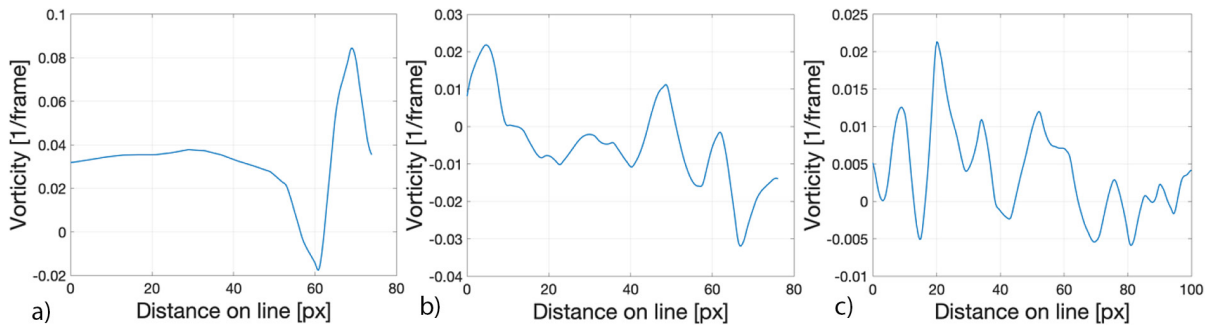


Fig. 16. Vorticity at the profile lines of the specimens: Specimen No. 1 (a), No. 2 (b), and No. 3 (c) Other derivatives that are useful to describe a flow are divergence (for example, see [37], [38]), and shear rate and strain rate (for example, see [36]).

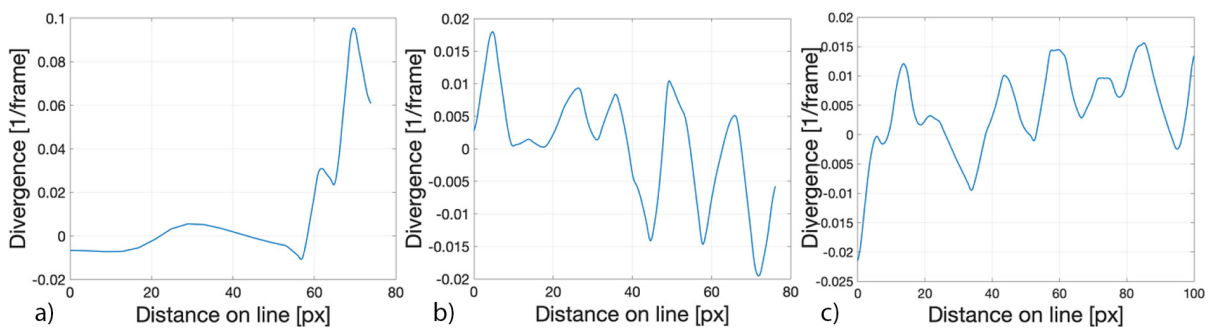


Fig. 17. Divergence at the profile lines of the specimens: Specimen No. 1 (a), No. 2 (b), and No. 3 (c)

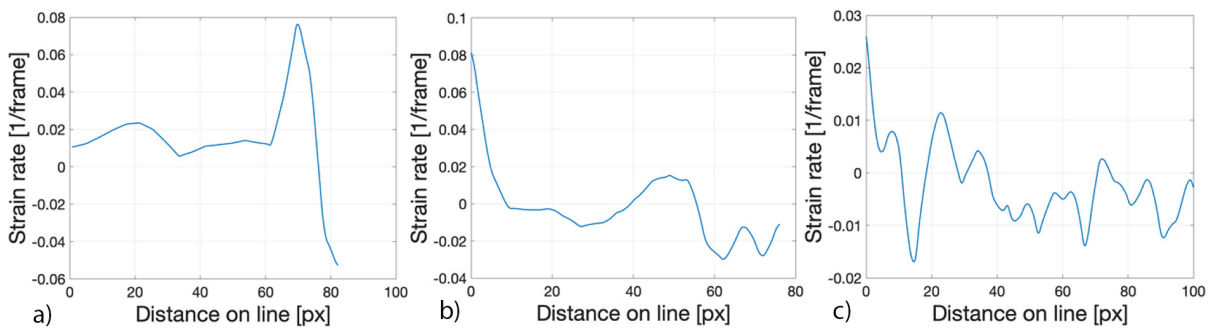


Fig. 18. Strain rate at the profile lines of the specimens respectively from left No. 1 (a) then No. 2 (b) and No. 3 (c)

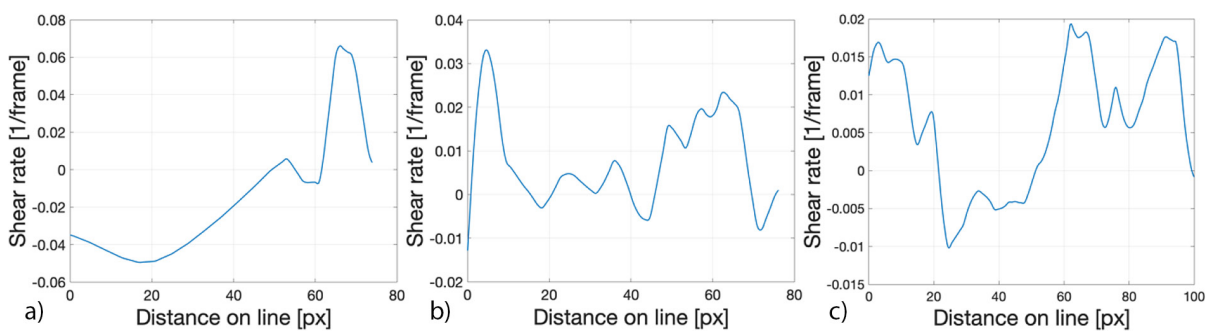


Fig. 19. Shear rate at the profile lines of the specimens: Specimen No. 1 (a), No. 2 (b), and No. 3 (c)

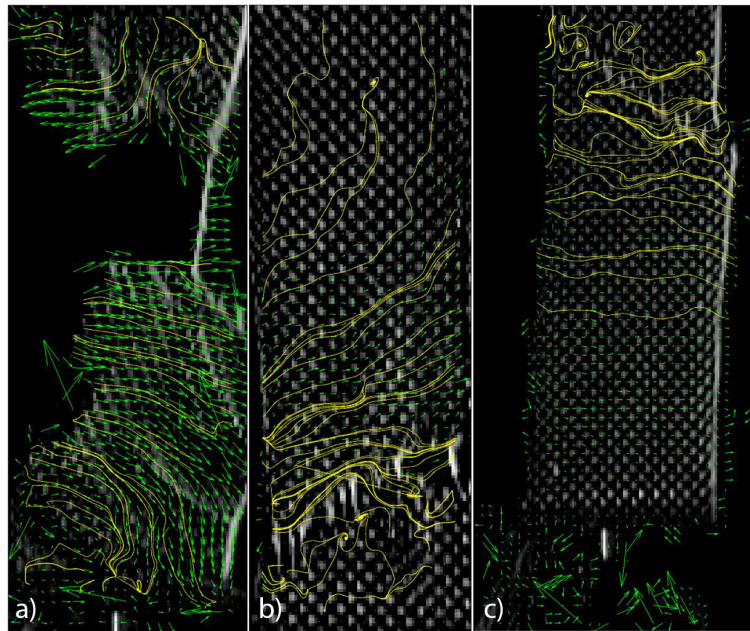


Fig. 20. Streamlines on the surfaces of the specimens

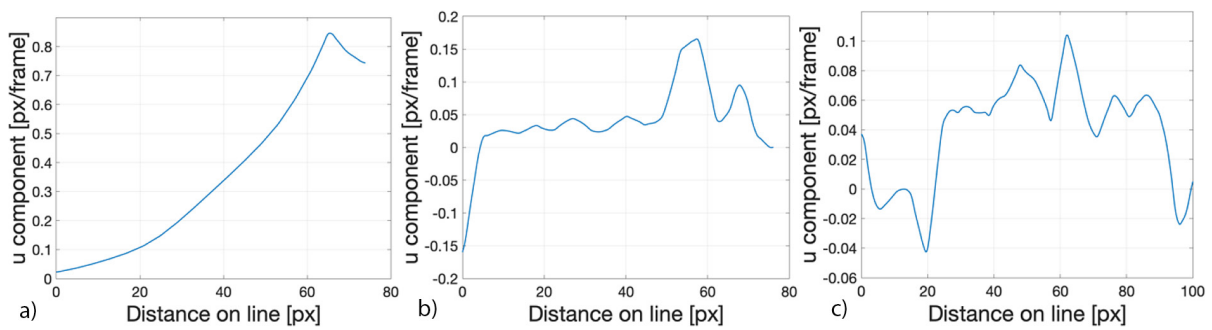


Fig. 21. U-component of the velocity of the movement at the profile lines of the specimens: Specimen No. 1 (a), No. 2 (b), and No. 3 (c)

[39], is that streamlines follow a circular pattern around the core, as demonstrated in Figure 20.

The velocity of the movement of the object on the surface can also be described by U (in the X direction) and V (in the Y direction) velocity components, respectively, as shown in Figure 21 and 22, respectively.

CONCLUSIONS

Tests conducted with the assistance of a fast camera can aid the visualisation of the complex composite behaviours of fabrics. They can help understand the mechanism of the damage to the fabric. Recorded fast camera films show effects

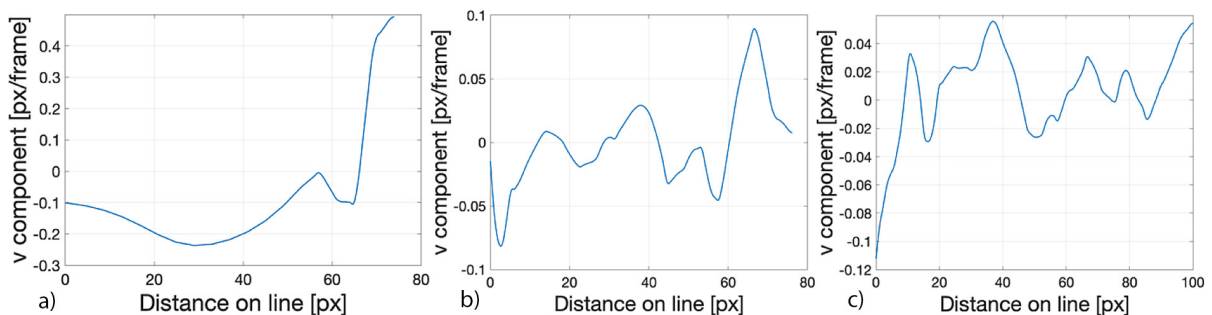


Fig. 22. V-component of the velocity of the movement at the profile lines of the specimens: Specimen No. 1 (a), No. 2 (b), and No. 3 (c)

that are not recorded in typical tests as well as in numerical analysis. The obtained results show the importance of clamping the specimens correctly in the grips of the strength machine. In this article, we presented a few examples that complement the conventional method of strength analysis of materials using a testing machine. The graphic data registered using the high-speed camera allowed us to characterise the changes occurring in the sample during the test in a spatial manner on the entire fabric surface and enabled access to many parameters at any given time of the movement. A well-known measurement method that is widely used in fluid mechanics, particle tracking and DPIV provided the opportunity to conduct a deeper analysis of the changes occurring in the sample during the test. The presented results prove that the seemingly simple phenomenon, which was so far commonly characterised by Young's modulus, can also be described using the adaptation of the DPIV method proposed in this paper.

REFERENCES

1. Tensile Structures (v. 1 & 2): Otto, Frei: 9780262650052: Amazon.com: Books. (n.d.). Retrieved from <https://www.amazon.com/Tensile-Structures-v-1-2/dp/0262650053> (accessed Jan. 04, 2021).
2. Zienkiewicz, O.C., Taylor, R.L., & Zhu, J.Z. (2020). The finite element method: Its basis and fundamentals. Sixth edition. Retrieved from <https://www.elsevier.com/books/the-finite-element-method-its-basis-and-fundamentals/zienkiewicz/978-0-08-047277-5> (accessed Jan. 04, 2021)
3. Kłonica M., Kuczmaszewski J., Samborski S (2015) Effect of a notch on impact resistance of the epidian 57/Z1 epoxy material after „thermal shock”. *Solid State Phenomena*, 240, 161–167.
4. Bielawski R., Rządkowski W., Kowalik M.P., Kłonica K. (2020) Safety of aircraft structures in the context of composite element connection. *International Review of Aerospace Engineering*, 13(5), 159–164.
5. Skoczylas J., Samborski S., Kłonica M. (2021) A multilateral study on the FRP Composite's matrix strength and damage growth resistance /*Composite Structures*, 63, 1–7.
6. ISO – ISO 1421:2017 – Rubber- or plastics-coated fabrics – Determination of tensile strength and elongation at break. Retrieved from <https://www.iso.org/standard/2146.html> (accessed Jan. 04, 2021)
7. Li, R., & Zhang, D. (2018). A visco-hyperelastic constitutive model for fiber-reinforced rubber composites. 33rd Technical Conference of the American Society for Composites, 5, 2957–2965. <https://doi.org/10.12783/asc33/26145>
8. Popov, L.N., Malanov, A.G., Slutsker, G.Y., & Stalevich, A.M. (1993). Viscoelastic properties of technical fabrics. *Fibre Chemistry*, 25(3), 211–214. <https://doi.org/10.1007/BF00551135>
9. Jekel, C.F., Venter, G., & Venter, M.P. (2017). Modeling PVC-coated polyester as a hypoelastic non-linear orthotropic material. *Composite Structures*, 161(161), 51–64. <https://doi.org/10.1016/j.compstruct.2016.11.019>
10. Van Craenenbroeck, M., Puystiens, S., De Laet, L., Van Hemelrijck, D., & Mollaert, M. (2015). Biaxial testing of fabric materials and deriving their material properties - A quantitative study. (accessed Jan. 04, 2021)
11. Van Craenenbroeck, M., Puystiens, S., De Laet, L., Van Hemelrijck, D., & Mollaert, M. (2016). Quantitative study of the impact of biaxial test protocols on the derived material parameters for a PVC coated polyester fabric. *Procedia Engineering*, 155, 220–229. <https://doi.org/10.1016/j.proeng.2016.08.023>
12. Ambroziak, A. (2015). Mechanical properties of Preconstraint 1202S coated fabric under biaxial tensile test with different load ratios. *Construction and Building Materials*, 80, 210–224. <https://doi.org/10.1016/j.conbuildmat.2015.01.074>
13. EN 17117-1:2018 – Rubber or plastics-coated fabrics – Mechanical test methods under biaxial stress states – Part 1: Tensile stiffness properties. Retrieved from <https://standards.iteh.ai/catalog/standards/cen/5cb3de61-8eee-4da6-bdf7-8dd2284a62e1/en-17117-1-2018> (accessed Jan. 04, 2021).
14. Van Craenenbroeck, M., Mollaert, M., & De Laet, L. (2019). The influence of test conditions and mathematical assumptions on biaxial material parameters of fabrics. *Engineering Structures*, 200, 109691. <https://doi.org/10.1016/j.engstruct.2019.109691>
15. Zerdzicki, K., Klosowski, P., & Woznica, K. (2019). Influence of service ageing on polyester-reinforced polyvinyl chloride-coated fabrics reported through mathematical material models. *Textile Research Journal*, 89(8), 1472–1487. <https://doi.org/10.1177/0040517518773374>
16. Monticelli, C., Carvelli, V., Fan, Z., Valletti, D., Nebiolo, M., & Messidoro, A. (2017). Biaxial Loading of a Textile Ribbons Structure for an Inflatable Module of Space Habitats. *Experimental Techniques*, 41(1), 9–17. <https://doi.org/10.1007/s40799-016-0150-5>
17. Shi, T., Hu, J., Chen, W., & Gao, C. (2020). Biaxial tensile behavior and strength of architectural fabric membranes. *Polymer Testing*, 82. <https://doi.org/10.1016/j.polymtest.2020.102311>

- org/10.1016/j.polymertesting.2019.106230
18. Xu, J., Zhang, Y., Wu, M., & Zhao, Y. (2020). A phenomenological material model for PTFE coated fabrics. *Construction and Building Materials*, 237. <https://doi.org/10.1016/j.conbuildmat.2019.117667>
 19. Ambroziak, A., & Klosowski, P. (2011). Review of constitutive models for technical woven fabrics in finite element analysis. *AATCC Review*, 11(3), 58–67.
 20. Ambroziak, A., & Klosowski, P. (2014). Mechanical properties for preliminary design of structures made from PVC coated fabric. *Construction and Building Materials*, 50, 74–81. <https://doi.org/10.1016/j.conbuildmat.2013.08.060>
 21. ISO – ISO 1421:2016 – Rubber- or plastics-coated fabrics – Determination of tensile strength and elongation at break. Retrieved from <https://www.iso.org/standard/65588.html> (accessed Jan. 10, 2021).
 22. Klosowski, P., Zerdzicki, K., & Woznica, K. (2019). Influence of artificial thermal ageing on polyester-reinforced and polyvinyl chloride coated AF9032 technical fabric. *Textile Research Journal*, 89(21–22), 4632–4646. <https://doi.org/10.1177/0040517519839934>
 23. Roushdy, M. (2006). Comparative study of edge detection algorithms applying on the grayscale noisy image using morphological filter Medical image classification using random forest View project Vision-Based Topological SLAM for Autonomous Robots View project. Retrieved from <http://cis.shams.edu.eg> (accessed Jan. 16, 2021).
 24. Mohan, V., Vijayarani, S., & Vinupriya, M.M. (2013). Performance analysis of canny and sobel edge detection algorithms in image mining privacy preserving data mining view project performance analysis of canny and sobel edge detection algorithms in image mining. Article in *International Journal of Innovative Research in Computer and Communication Engineering*, 3297. Retrieved from www.ijirccce.com (accessed Jan. 16, 2021).
 25. Gao, W., Zhang, X., Yang, L., & Liu, H. (2010). An improved Sobel edge detection. 2010 3rd International Conference on Computer Science and Information Technology, 5, 67–71. <https://doi.org/10.1109/ICCSIT.2010.5563693>
 26. Kanopoulos, N., Vasanthavada, N., & Baker, R. L. (1988). Design of an image edge detection filter using the Sobel operator. *IEEE Journal of Solid-State Circuits*, 23(2), 358–367. <https://doi.org/10.1109/4.996>
 27. Aqrabi, A.A., & Boe, T.H. (2011). Improved fault segmentation using a dip guided and modified 3D Sobel filter. *SEG Technical Program Expanded Abstracts*, 30(1), 999–1003. <https://doi.org/10.1190/1.3628241>
 28. McIlhagga, W. (2018). Estimates of edge detection filters in human vision. *Vision Research*, 153, 30–36. <https://doi.org/10.1016/j.visres.2018.09.007>
 29. Shrivakshan, G.T., & Chandrasekar, C. (2012). A Comparison of various edge detection techniques used in image processing. Retrieved from www.IJCSI.org (accessed Jan. 16, 2021).
 30. PIVlab – Towards User-friendly, Affordable and Accurate Digital Particle Image Velocimetry in MATLAB. Retrieved from <https://openresearch-software.metajnl.com/articles/10.5334/jors.bl/> (accessed Jan. 10, 2021).
 31. Thielicke, W., & Stamhuis, E.J. (2014). PIVlab – towards user-friendly, affordable and accurate digital particle image velocimetry in MATLAB. *Journal of Open Research Software*, 2(1). <https://doi.org/10.5334/jors.bl>
 32. Thielicke. (2014). *The Flapping Flight of Birds*. [S.n.].
 33. Thielicke. (n.d.). Digital Particle Image Velocimetry. Retrieved from <http://pivlab.blogspot.com>
 34. Utami, T., Blackwelder, R.F., & Ueno, T. (1991). A cross-correlation technique for velocity field extraction from particulate visualization. *Experiments in Fluids*, 10(4), 213–223. <https://doi.org/10.1007/BF00190391>
 35. Huang, H., Dabiri, D., & Gharib, M. (1997). On errors of digital particle image velocimetry. *Measurement Science and Technology*, 8(12), 1427–1440. <https://doi.org/10.1088/0957-0233/8/12/007>
 36. Stamhuis, E.J., & Videler, J.J. (1995). Quantitative flow analysis around aquatic animals using laser sheet particle image velocimetry. *Journal of Experimental Biology*, 198(2), 283–294. Retrieved from <https://pubmed.ncbi.nlm.nih.gov/9317812/> (accessed Jan. 10, 2021).
 37. Nauwelaerts, S., Stamhuis, E.J., & Aerts, P. (2005). Propulsive force calculations in swimming frogs I. A momentum-impulse approach. *Journal of Experimental Biology*, 208(8), 1435–1443. <https://doi.org/10.1242/jeb.01509>
 38. Stamhuis, E.J., & Nauwelaerts, S. (2005). Propulsive force calculations in swimming frogs II. Application of a vortex ring model to DPIV data. *Journal of Experimental Biology*, 208(8), 1445–1451. <https://doi.org/10.1242/jeb.01530>
 39. Robinson, S.K., & Kline, S.J. (1989). A review of quasi-coherent structures in a numerically simulated turbulent boundary layer. Retrieved from <https://ntrs.nasa.gov/api/citations/19900004407/downloads/19900004407.pdf> (accessed Jan. 10, 2021).